APS physics

CHORUS

This is the accepted manuscript made available via CHORUS. The article has been published as:

Stabilization of magnetic skyrmions by uniaxial tensile strain

S. Seki, Y. Okamura, K. Shibata, R. Takagi, N. D. Khanh, F. Kagawa, T. Arima, and Y. Tokura

Phys. Rev. B **96**, 220404 — Published 19 December 2017

DOI: 10.1103/PhysRevB.96.220404

Stabilization of magnetic skyrmions by uniaxial tensile strain

S. Seki[1*], Y. Okamura[2], K. Shibata[1], R. Takagi[1], N. D. Khanh[1], F. Kagawa[1], T. Arima[1,3], Y. Tokura[1,2]

[1]*RIKEN Center for Emergent Matter Science (CEMS), Wako 351-0198, Japan*

[2]*Department of Applied Physics and Quantum Phase Electronics Center (QPEC), University of Tokyo, Tokyo 113-8656, Japan*

[3]*Department of Advanced Materials Science, University of Tokyo, Kashiwa 277-8561, Japan*

Abstract

Magnetic skyrmion with topological particle nature has recently attracted attention as a potential information carrier for novel magnetic storage device. For single-phase bulk crystals, skyrmions usually appear for a very narrow temperature region just below magnetic ordering temperature T_c, and the stabilization of skyrmions for wider temperature range remains an important challenge. Here, by investigating the impact of uniaxial tensile stress for a chiral magnet Cu_2OSeO_3, we demonstrate that only less than 0.2% of uniaxial elongation can dramatically stabilize skyrmions for whole temperature range from T_c to the lowest temperature. The stability of skyrmions essentially depends on the geometrical relationship among the directions of strain, magnetic field, and crystallographic axes, which is consistently explained in terms of the anisotropic modulation of Dzyaloshinskii-Moriya interaction and magnetocrystalline anisotropy. Our finding may provide a good strategy for materials design to enhance the skyrmion stability.

Skyrmion is a concept describing the topologically-protected excitation with particle nature[1], which appears as a nanometric vortex-like swirling spin texture in magnetic materials (Fig. 1(i))[2–5]. Magnetic skyrmions are characterized by the unique manner of interaction with external electric field, through the quantum Berry phase in metallic systems[6–9] or relativistic spin-orbit interaction in insulating systems[10, 11]. Due to their electric controllability, particle nature and small size, skyrmions are intensively studied as the potential information carrier for novel magnetic storage with high information density and energy efficiency[12–14].

Skyrmions are generally stabilized by Dzyaloshinskii-Moriya (DM) interaction, i.e. antisymmetric exchange interaction emerging under the noncentrosymmetric environments[2, 3, 5]. In case of the single-phase compounds, the formation of skyrmions has mostly been reported for a series of magnetic materials with chiral cubic crystal structure, such as metallic B20 alloys ($T_c \sim 280$ K)[3, 15, 17] and Co-Zn-Mn alloys ($T_c \sim 400$ K)[16] or insulating Cu_2OSeO_3 ($T_c = 58$ K)[10], all of which are characterized by similar H(magnetic field)-T(temperature) magnetic phase diagrams as shown in Fig. 1(f). However, the bulk crystals of these compounds host skyrmions only for a very narrow temperature region just below the magnetic ordering temperature T_c, and the stabilization of skyrmions for a wider temperature range is essential for their application. For this purpose, several different approaches have been proposed. For example, the employment of thin-film sample thinner than the magnetic modulation period (< 100 nm) can stabilize the skyrmion state for the out-of-plane magnetic field[18], but this approach is not applicable to the arbitral shape of crystal. Another potential strategy is the application of uniaxial pressure[19–21], hydrostatic pressure[22, 23] or electric field[24]. However, their reported magnitude of modulation in T_{c2} (i.e. lower critical temperature of the skyrmion state) usually remains just in the order of several Kelvin, and the stabilization of skyrmions for the whole temperature range from T_c to zero temperature has never been achieved. Note that the rapid cooling of the sample can often create the supercooled skyrmion state[24–26], while this corresponds to the metastable state with finite lifetime and not the thermal-equilibrium ground state.

In this Rapid Communication, we report the dramatic stabilization of the skyrmion state by minimal uniaxial tensile strain for the prototypical chiral-lattice insulator Cu_2OSeO_3 with cubic crystal structure. The observed strain-induced modulation of T_{c2} is one order of magnitude larger than the previous reports for MnSi with uniaxial compressive strain[20, 21],

and we found that only less than 0.2% of uniaxial lattice elongation is sufficient to stabilize the SkX state down to the lowest temperature. The stability of the skyrmion state essentially depends on the geometrical relationship among the directions of uniaxial strain, magnetic field and crystallographic axes, which can be consistently explained in terms of the strain-induced modulation of DM interaction and magnetocrystalline anisotropy.

The schematic illustration of the device structure employed in this study is shown in Fig. 1(a). Here, we fabricated two different type of devices; The plate-shaped Cu_2OSeO_3 single crystal with the thickness of 1 μm was fixed to Si substrate by W (tungsten) bonding at one (Fig. 1(b)) or both (Fig. 1(c)) side edges at room temperature. Only in the latter case, the uniaxial tensile strain σ is applied to Cu_2OSeO_3 due to the mismatch of thermal expansion coefficients at low temperatures, as confirmed by the simulation of thermal strain given in the supplementary materials (Fig. S1(d))[27]. Figure 1(d) indicates the reported temperature dependence of lattice constant for Si[35] and Cu_2OSeO_3[36], which suggests that the strained Cu_2OSeO_3 sample is elongated along the bridging direction by 0.12% and this value remains almost constant below $T_c = 58$ K. As discussed later, the identification of magnetic phase is possible through the analysis of magnetic resonance modes[37–40]. For this purpose, the Au coplanar waveguide was fabricated on the substrate, which enables the measurement of microwave absorption spectra ΔS_{11} associated with the magnetic resonance in Cu_2OSeO_3 by a vector network analyzer.

First, we briefly discuss the H-T phase diagram for the unstrained Cu_2OSeO_3 sample (Fig. 1(f)) in the device form shown in Fig. 1(b), which well reproduces the ones reported in Refs. [10, 39, 40]. According to the previous neutron diffraction experiments[41, 42], the helical magnetic order is realized at $H = 0$, where the neighboring spins rotate within a plane normal to the magnetic modulation vector q (Fig. 1(g)). While this q-vector is weakly pinned to the $\langle 001 \rangle$ axes by magnetocrystalline anisotropy, the application of external magnetic field reorients q along the H-direction (i.e. $H \parallel q$) and stabilizes the conical magnetic structure as shown in Fig. 1(h). The further increase of H induces the transition into the collinear ferromagnetic state. The SkX (i.e. triangular lattice of skyrmion) state (Fig. 1(i)), characterized by triple q-vectors normal to external magnetic field (i.e. $H \perp q$), appears for the narrow H-T region just below T_c.

Figure 1(e) indicates the theoretically predicted H-dependence of magnetic resonance frequency for various magnetic phases[37], which has experimentally been verified for

Cu_2OSeO_3 in Refs. [37, 39, 40]. The ferromagnetic state generally hosts a single magnetic resonance mode, whose frequency shows H-linear increase. On the other hand, the helical or conical spin states host two resonance modes (i.e. the +Q and -Q modes, the latter of which is located at lower frequency with much weaker absorption intensity) and their frequency gradually decreases as a function of H[37, 43]. The SkX state also hosts two resonance modes, i.e. the clockwise (CW) and counter-clockwise (CCW) rotational modes, where the CCW mode is characterized by lower frequency and stronger absorption intensity[37, 38]. Importantly, the resonance frequency of the CCW mode monotonically increases against H, which enables the clear distinction of the SkX state from the helical or conical state.

On the basis of the above knowledge, we investigated the H-T phase diagram for the Cu_2OSeO_3 sample with the uniaxial tensile strain σ, using the device shown in Fig. 1(c). First, we discuss the case with the in-plane H applied normal to the σ-direction (Fig. 2(b)). Figures 2(c) and (e) indicate the H-dependence of microwave absorption spectra ΔS_{11} at 48 K. Between 23 mT and 43 mT, two resonance modes are identified, where the lower-lying mode shows stronger microwave absorption and its frequency increases as a function of H. These features are consistent with the theoretical prediction for the SkX state (Fig. 1(e))[37, 38], and the observed modes can be assigned as the CW and CCW modes of skyrmions. Except for this H-region, the resonance frequency shows negative (positive) slope against H below (above) 53 mT, which represents the helical/conical (ferromagnetic) state. Note that the -Q mode in the helical/conical state is too weak to be detected, in accord with the theory[37]. In Figs. 2(d) and (f), we also plotted the corresponding data measured at 10 K. Notably, at this low temperature, the SkX state hosting the CW and CCW modes with similar characters appears between 30 mT and 48 mT, and the discontinuous change of resonance frequency is observed upon the transition into the ferromagnetic state. Figure 2(a) summarizes the H-T phase diagram for the configuration shown in Fig. 2(b), with the background color representing the peak intensity of the CCW mode in the ΔS_{11} spectra. The comparison of Fig. 1(f) and Fig. 2(a) clearly demonstrates that the application of uniaxial tensile strain dramatically stabilizes the SkX state, even down to the lowest temperature.

The stability of the SkX state largely depends on the directional relationship between H and σ. On the basis of the T- and H-variation of the magnetic resonance modes, the H-T phase digram obtained with the in-plane H parallel to σ is indicated in Fig. 3(a). In

this configuration, the SkX state is rather destabilized and completely disappears from the phase diagram. On the other hand, with the out-of-plane H normal to σ, the SkX state is moderately stabilized down to 43 K (Fig. 3(b)) (See Fig. S2 in supplementary materials for the raw data of $|\Delta S_{11}|$ spectra[27]). The above results suggest that the SkX state becomes more stable for $H \perp \sigma$, and unstable for $H \parallel \sigma$. Intuitively, these behaviors can be understood by considering the σ-induced pinning of magnetic modulation vector q[20, 21]. In Figs. 3(c) and (d), we plotted the H-dependence of absorption spectra at 34 K for the $H \parallel \sigma$ and $H \perp \sigma$ setups, respectively. In the latter configuration, the discontinuous change of resonance frequency is observed at 80 mT, which corresponds to the transition between the helical and conical spin state, i.e. the reorientation of q-vector along the H-direction. In contrast, such an anomaly is absent in the former $H \parallel \sigma$ setup (Fig. 3(c)), suggesting that the helical q-vector is pinned along the $\sigma \parallel [001]$ direction under zero magnetic field for Cu_2OSeO_3. To sustain such $\sigma \parallel q$ relationship, the SkX ($H \perp q$) state can be stabilized and destabilized against the competing conical ($H \parallel q$) spin state under the $H \perp \sigma$ and $H \parallel \sigma$ configurations, respectively.

To further discuss the microscopic origin of these phenomena, we investigated the stability of the SkX state as a function of the angle (θ_H) between the in-plane H-direction and σ-direction (Fig. 3(e)). In Fig. 3(f), the maximum absorption intensity of the CCW mode at each temperature is plotted against θ_H. At $\theta_H = 60°$, the SkX state appears between 55 K and 58 K, and its stability is almost comparable with the case for the unstrained sample. By increasing and decreasing θ_H from this value, the SkX state becomes more stable and unstable, respectively. These behaviors can be well reproduced by considering the anisotropic modulation of magnetocrystalline anisotropy and/or DM interaction by the uniaxial tensile strain. In case of the chiral cubic crystal structure, the uniaxial lattice elongation along the z-direction causes the emergence of additional free energy term $\Delta_{\mathrm{K}} = -K_z m_z^2$ and $\Delta_{\mathrm{DM}} = -d_z|m_y(\partial m_x/\partial z) - m_x(\partial m_y/\partial z)|$, which correspond to the contribution from magnetocrystalline anisotropy and DM interaction, respectively[19, 44]. Here, K_z and d_z represent the magnitude of each stained-induced term, and $m_i (i = x, y, z)$ is the local magnetization component along the i-direction. By considering the observed pinning of the helical q-vector along the σ-direction, the sign of K_z and d_z should be negative and positive, respectively. The strain-induced energy shift of each magnetic phase can be estimated by calculating $\langle \Delta_{\mathrm{K}} \rangle = \int \Delta_{\mathrm{K}} d\vec{r} / \int d\vec{r}$ and $\langle \Delta_{\mathrm{DM}} \rangle = \int \Delta_{\mathrm{DM}} d\vec{r} / \int d\vec{r}$, where the integral is taken

over each magnetic unit cell. Figures 3(g) and (h) indicate the θ_H-dependence of $\langle\Delta_{\rm K}\rangle$ and $\langle\Delta_{\rm DM}\rangle$ calculated for the SkX and conical states (See supplementary materials for the detail of calculation and the direct experimental evaluation of K_z and d_z[27]). Both terms stabilize (destabilize) the SkX state for θ_H larger (smaller) than the critical value around 60°, well reproducing the experimental observation in Fig. 3(f).

In Fig. 4(e), the H-T phase diagrams for the strained and unstrained Cu_2OSeO_3, measured with various directional combinations of H and σ under different crystallographic orientations, are summarized. In case of the unstrained Cu_2OSeO_3, the SkX state appears between 56 K and 58 K for any H-direction reflecting the cubic symmetry of the original crystal structure (Fig. 4(c))[41, 45]. By applying $\sigma \parallel H$, the SkX state is always suppressed (Fig. 4(d)). In contrast, the application of $\sigma \perp H$ generally enhances the stability of the SkX state. Here, the SkX state is stabilized down to the lowest temperature for the in-plane H normal to σ (Fig. 4(a)), while the lower critical temperature T_{c2} for the SkX state is of the order of 40 K for the out-of-plane H normal to σ (Fig. 4(b)). In general, magnetic dipole-dipole interaction favors to orient the magnetization along the in-plane direction. Under the out-of-plane H, the conical spin state has larger in-plane spin component than the SkX state, which may explain the relatively limited degree of the SkX stabilization in this experimental geometry. Notably, for the configuration with $\sigma \parallel [110]$ and $H \parallel [1\bar{1}0]$, such σ-induced stabilization of the SkX state does not happen. Since the q-vector favors to orient along the $\langle 100\rangle$ axes in the unstrained Cu_2OSeO_3[41, 42], the application of $\sigma \parallel [110]$ probably selects the $q \parallel \langle 100\rangle$ closest to σ-direction (i.e. $q \parallel [100]$ and $q \parallel [010]$) rather than realizing the $q \parallel \sigma$ configuration. In this situation, the stable q-directions do not exist within the $H \perp q$ plane for $H \parallel [1\bar{1}0]$, therefore the stability of the SkX state is not enhanced. This result suggests that the appropriate choice of the crystallographic orientation is also important for the σ-induced control of the SkX stability.

In this work, we experimentally demonstrated that uniaxial elongation only by 0.2% in the isotropic chiral magnet can dramatically stabilize the skyrmion state for whole temperature range from T_c to the lowest temperature. Note that some metallic B20 alloys such as MnSi[20, 21] and FeGe[44] are reported to host the opposite sign of K_z or d_z from the current case with insulating Cu_2OSeO_3, and further investigation of the relationship between the electronic band structure and the magnitude/sign of strain effect, in particular for other chiral-lattice magnets with higher-T_c, would be an interesting issue[46]. Our present findings

also provide a strategy of materials design toward the enhancement of the SkX stability at ambient pressure, since similar magnitude of lattice symmetry reduction is often possible through chemical substitution approaches such as the tolerance factor tuning[47] or the introduction of Jahn-Teller active ion[48]. Considering the present fact that the skyrmion lattice is stabilized within the anisotropic two dimensional plane including the σ-axis, the noncentrosymmetric magnets without the isotropic two dimensional plane, such as the ones with orthorhombic or monoclinic crystal lattice symmetry, may also be the promising candidate to realize the skyrmions with enhanced stability.

The authors thank N. Nagaosa, Y. Iwasa, M. Kawasaki, Y. Otani, K. Kondou, Y. Nii, M. Nakamura, T. Nakajima, N. Kanazawa, T. Kurumaji, D. Morikawa for enlightening discussions and experimental helps. This work was partly supported by the Mitsubishi Foundation, Grants-In-Aid for Scientific Research (Grants No. 17H05186 and No. 16K13842) from JSPS, and PRESTO from JST.

[1] T. H. R. Skyrme, Nucl. Phys. **31**, 556 (1962).

[2] A. N. Bogdanov, D. A. Yablonskii, Sov. Phys. JETP **68**, 101 (1989).

[3] S. Mühlbauer *et al.*, Science **323**, 915 (2009).

[4] X. Z. Yu, Y. Onose, N. Kanazawa, J. H. Park, J. H. Han, Y. Matsui, N. Nagaosa, Y. Tokura, Nature **465**, 901 (2010).

[5] U. K. Rößler, A. N. Bogdanov, C. Pfleiderer, Nature **442**, 797 (2006).

[6] A. Neubauer, C. Pfleiderer, B. Binz, A. Rosch, R. Ritz, P. G. Niklowitz, and P. Böni, Phys. Rev. Lett. **102**, 186602 (2009).

[7] F. Jonietz, S. Mühlbauer, C. Pfleiderer, A. Neubauer, W. Münzer, A. Bauer, T. Adams, R. Georgii, P. Böni, R. A. Duine, K. Everschor, M. Garst, and A. Rosch, Science **330**, 1648 (2010).

[8] X. Z. Yu, N. Kanazawa, W.Z. Zhang, T. Nagai, T. Hara, K. Kimoto, Y. Matsui, Y. Onose, and Y. Tokura, Nature Commun. **3**, 988 (2012).

[9] T. Schulz, R. Ritz, A. Bauer, M. Halder, M. Wagner, C. Franz, C. Pfleiderer, K. Everschor, M. Garst, and A. Rosch, Nature Phys. **8**, 301 (2012).

[10] S. Seki, X. Z. Yu, S. Ishiwata, Y. Tokura, Science **336**, 198 (2012).

[11] S. Seki, S. Ishiwata, Y. Tokura, Phys. Rev. B **86**, 060403(R) (2012).

[12] A. Fert, V. Cros, J. Sampaio, Nature Nanotech. **8**, 152 (2013).

[13] N. Nagaosa, Y. Tokura, Nature Nanotech. **8**, 899 (2013).

[14] S. Seki, M. Mochizuki, *Skyrmions in Magnetic Materials* (Springer, 2015).

[15] W. Münzer *et al.*, Phys. Rev. B **81**, 041203(R) (2010).

[16] Y. Tokunaga *et al.*, Nature Comm. 6, 7638 (2015).

[17] H. Wilhelm, M. Baenitz, M. Schmidt, U. K. Rößler, A. A. Leonov, and A. N. Bogdanov, Phys. Rev. Lett. **107**, 127203 (2011).

[18] X. Z. Yu, N. Kanazawa, Y. Onose, K. Kimoto, W. Z. Zhang, S. Ishiwata, Y. Matsui, and Y. Tokura, Nature Mater. **10**, 106 (2011).

[19] A. B. Butenko, A. A. Leonov, U. K. Rößler, A. N. Bogdanov *et al.*, Phys. Rev. B **82**, 052403 (2010).

[20] Y. Nii *et al.*, Nature Comm. **6**, 8539 (2015).

[21] A. Chacon *et al.*, Phys. Rev. Lett. **115**, 267202 (2015).

[22] R. Ritz, M. Halder, M. Wagner, C. Franz, A. Bauer, C. Pfleiderer, Nature **497**, 231 (2013)

[23] I. Levatić *et al.*, Sci. Rep. **6**, 21347 (2016).

[24] Y. Okamura *et al.*, Nature Comm. **7**, 12669 (2016).

[25] H. Oike *et al.*, Nature Phys. **12**, 62 (2016).

[26] K. Karube *et al.*, Nature Mater. **15**, 1237 (2016).

[27] See Supplemental Material at **URL** for the detail, which includes Refs. [28–34].

[28] K. H. Miller, X. S. Xu, H. Berger, E. S. Knowles, D. J. Arenas, M. W. Meisel, D. B. Tanner, Phys. Rev. B **82**, 144107 (2010).

[29] P. Auerkari, VTT Manufacturing Technology, Research Notes 1792 (1996).

[30] A. Nasekovskii, Sov. Phys. J. **12**, 65 (1969).

[31] P. Bak, M. H. Jensen, J. Phys. C: Solid St. Phys. **13**, L881 (1980).

[32] D. Cortés-Ortuño, P. Landeros, J. Phys.: Condens. Matter **25**, 156001 (2013).

[33] D. D. Stencil, *Theory of Magnetostatic Waves* (Springer, 1993).

[34] A. G. Gurevich, G. A. Melkov, *Magnetization Oscillations and Waves* (CRC Press, 1996).

[35] D. N. Batchelder, R. O. Simmons, J. Chem. Phys. **41**, 2324 (1964).

[36] J. G. Bos, C. V. Colin, T. T. M. Palstra, Phys. Rev. B **78**, 094416 (2008).

[37] T. Schwarze, J. Waizner, M. Garst, A. Bauer, I. Stasinopoulos, H. Berger, C. Pfleiderer, D.

Grundler, Nature Mater. **14**, 478 (2015).

[38] M. Mochizuki, Phys. Rev. Lett. **108**, 017601 (2012).

[39] Y. Onose, Y. Okamura, S. Seki, S. Ishiwata, Y. Tokura, Phys. Rev. Lett. **109**, 037603 (2012).

[40] Y. Okamura, F. Kagawa, M. Mochizuki, M. Kubota, S. Seki, S. Ishiwata, M. Kawasaki, Y. Onose, Y. Tokura, Nature Comm. **4**, 2391 (2013).

[41] T. Adams, A. Chacon, M. Wagner, A. Bauer, G. Brandl, B. Pedersen, H. Berger, P. Lemmens, C. Pfleiderer, Phys. Rev. Lett. **108**, 237204 (2012).

[42] S. Seki, J.-H. Kim, D. S. Inosov, R. Georgii, B. Keimer, S. Ishiwata, Y. Tokura, Phys. Rev. B **85**, 220406 (2012).

[43] M. Kataoka, J. Phys. Soc. Jpn. **56**, 3635 (1987).

[44] K. Shibata *et al.*, Nature Nanotech. **10**, 589 (2015).

[45] H. Effenberger, F. Pertlik, Monatsch. Chem. **117**, 887 (1986).

[46] T. Koretsune, N. Nagaosa, R. Arita, Sci. Rep. **5**, 13302 (2015).

[47] V. M. Goldschmidt, Naturwissenschaften, **14**, 477 (1926).

[48] H. Jahn, E. Teller, Proc. R. Soc. London, Ser. A **161**, 220 (1937).

Figures

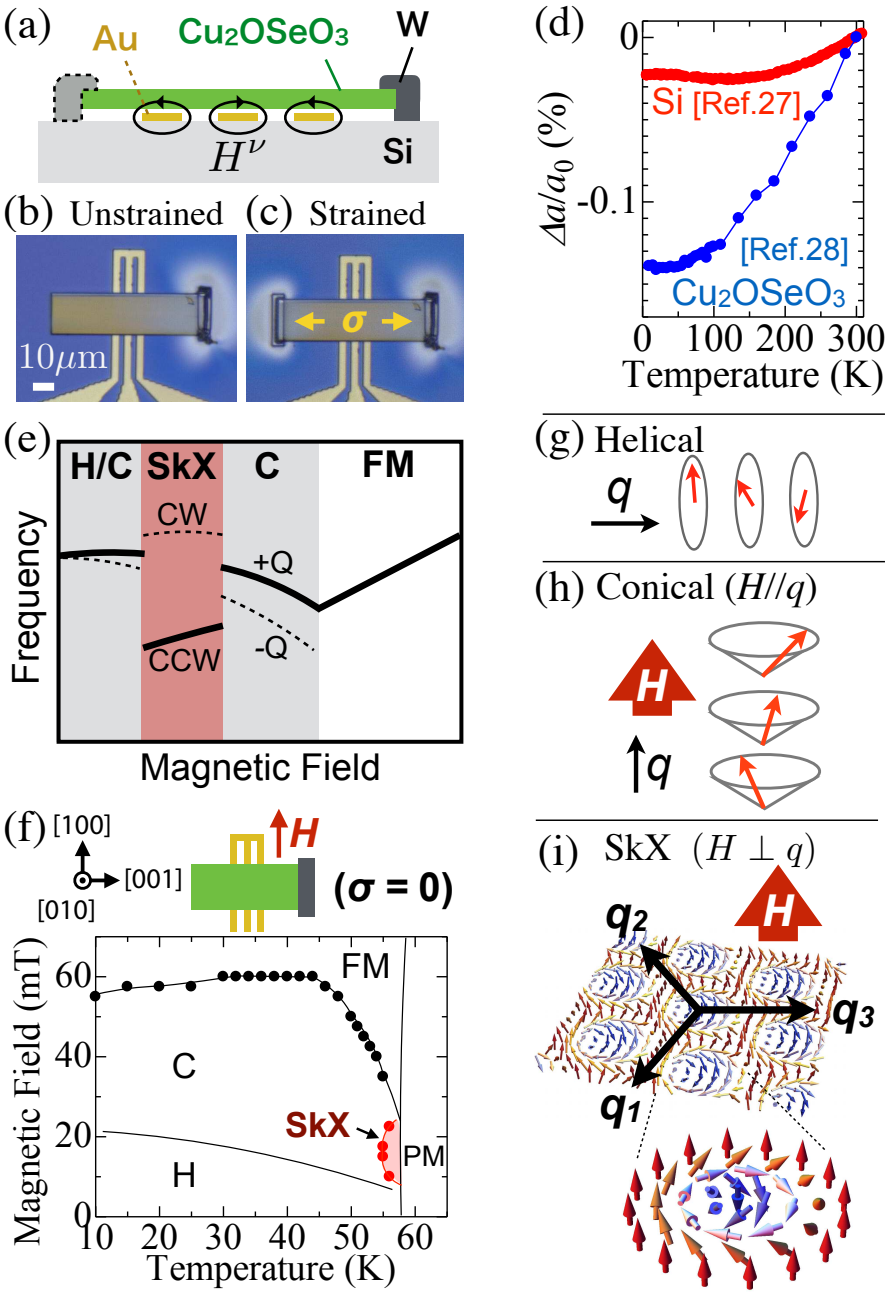
(a)
Au
Cu2OSeO3
W
Si
H^ν
(b) Unstrained
(c) Strained
10μm
σ
(d)
0
-0.1
Δa/a0 (%)
Si [Ref.27]
[Ref.28]
Cu2OSeO3
0 100 200 300
Temperature (K)
(e)
H/C
SkX
C
FM
CW
CCW
+Q
-Q
Frequency
Magnetic Field
(f)
[100]
[001]
[010]
H
(σ = 0)
60
40
20
0
FM
C
SkX
PM
H
Magnetic Field (mT)
10 20 30 40 50 60
Temperature (K)
(g) Helical
q
(h) Conical (H//q)
H
q
(i) SkX (H ⊥ q)
H
q2
q3
q1

FIG. 1: (a) Schematic side-view illustration of device structure for magnetic resonance experiments. (b),(c) The corresponding top-view optical images of unstrained and strained samples. (d) Temperature dependence of lattice constant a for Si and Cu_2OSeO_3, previously reported in Refs. [35, 36]. a_0 and Δa correspond to a at 300 K and $a - a_0$, respectively. (e) Magnetic field dependence of magnetic resonance frequency for the modes active in the $H \perp H^\nu$ configuration (with H^ν representing the oscillating magnetic field component of microwave) theoretically predicted in Ref. [37]. The modes described with dashed lines are expected to cause weaker microwave absorption than the ones with solid lines. (f) H-T phase diagram for unstrained Cu_2OSeO_3, obtained with the device shown in (b). In (e) and (f), H, C, SkX, FM, and PM represent helical, conical, skyrmion lattice, ferromagnetic, and paramagnetic spin states, respectively. (g)-(i) Schematic illustration of helical, conical, and skyrmion lattice spin textures, respectively.

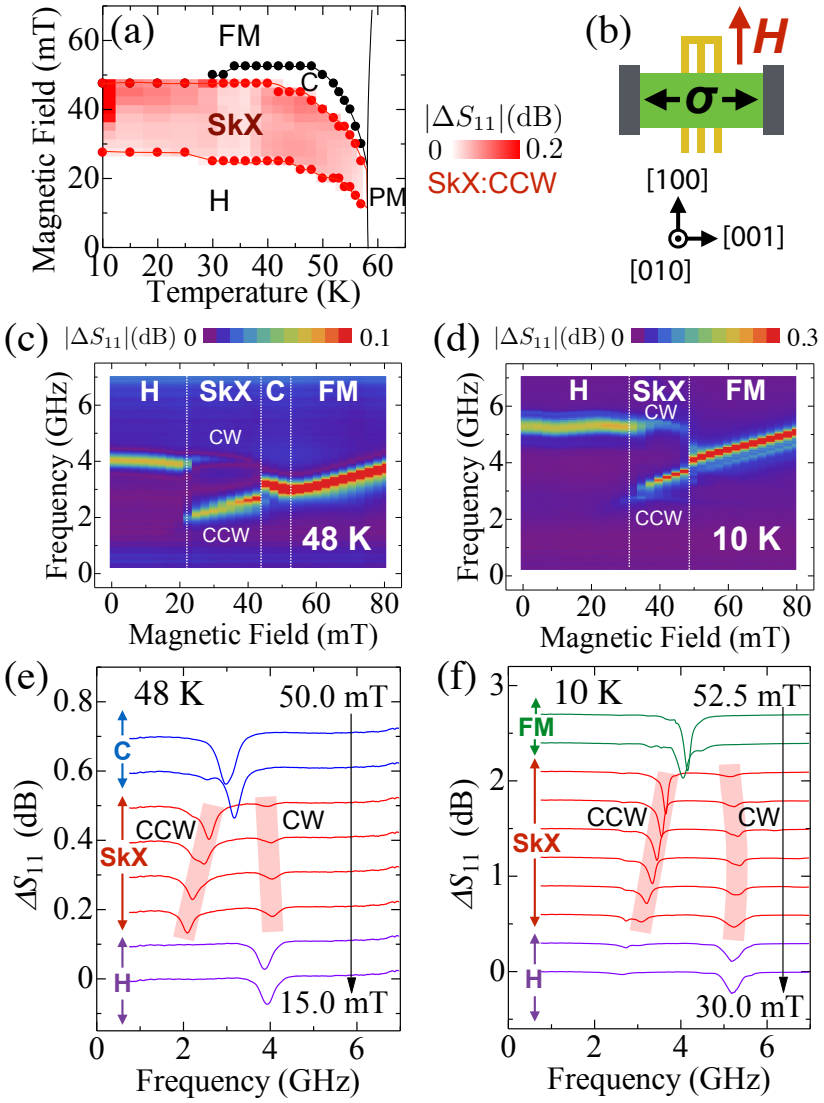

FIG. 2: Stabilization of skyrmion state for Cu_2OSeO_3 with uniaxial tensile strain. (a) H-T phase diagram for Cu_2OSeO_3 with uniaxial tensile strain σ, obtained with the device shown in Fig. 1(c). Here, in-plane H is applied normal to σ, and the corresponding measurement geometry is shown in (b). Background color represents the microwave absorption intensity $|\Delta S_{11}|$ of the CCW mode in the the SkX state. (c),(d) Magnetic field dependence of microwave absorption spectra, obtained at 48 K and 10 K, respectively. Background color represents the magnitude of microwave absorption, and the raw data of absorption spectra for selected magnetic field values at each temperature are shown in (e) and (f).

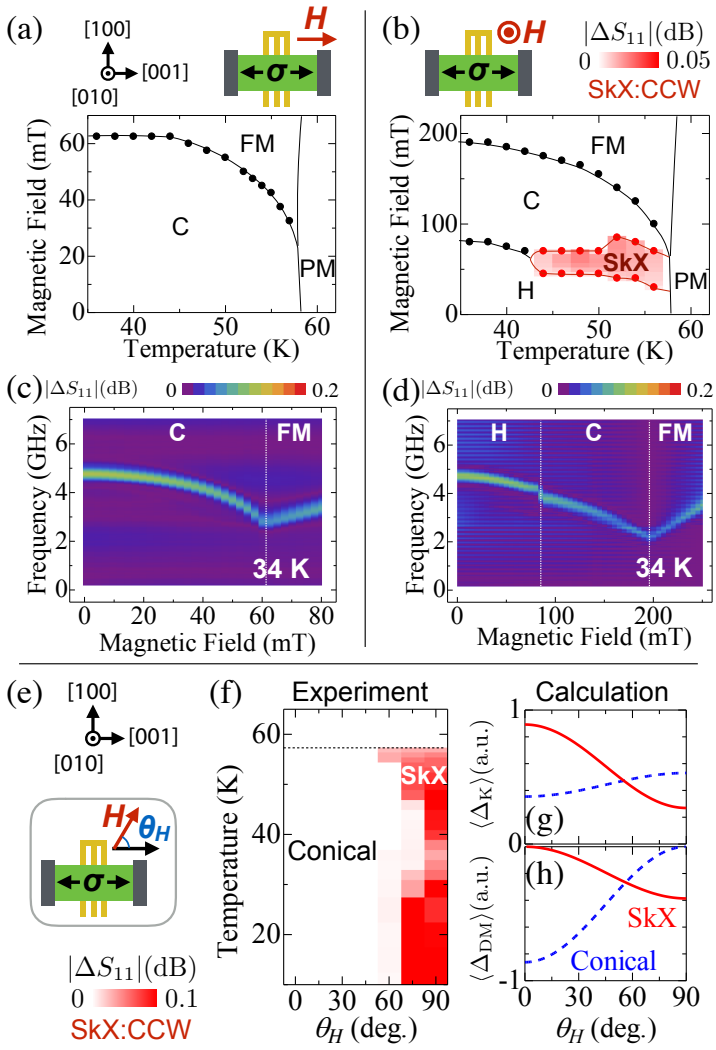

FIG. 3: Skyrmion stability under various directional combinations of H and σ, obtained with the device shown in Fig. 1(c). (a),(b) H-T phase diagrams for Cu_2OSeO_3 with uniaxial tensile strain σ, obtained under the in-plane H parallel to σ and the out-of-plane H normal to σ, respectively. (c),(d) Magnetic field dependence of microwave absorption spectra, measured at 34 K for each experimental configuration. (e) Schematic illustration of the definition of θ_H, which corresponds to the angle between the in-plane H and σ directions. (f) Experimentally obtained θ_H-dependence of skyrmion stability. Background color represents maximum absorption intensity of the CCW mode in the SkX state at each temperature. $\theta_H = 0°$ and $\theta_H = 90°$ correspond to Fig. 3(a) and Fig. 2(a), respectively. (g),(h) θ_H-dependence of free energy terms $\langle \Delta_{\rm K} \rangle$ and $\langle \Delta_{\rm DM} \rangle$, respectively, calculated for the SkX and conical spin states. Here, we assumed that H-induced magnetization takes a half of the saturation value.

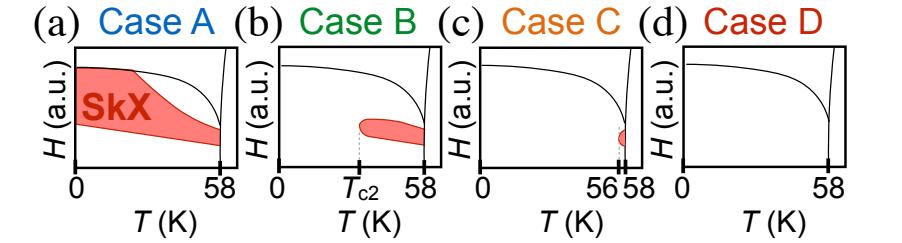

(e)	Axes	→H	↑H	⊙H
σ	[100] [010] [001]	D	A	B (T_{c2} = 43)
σ	[110] [1$\bar{1}$0] [001]	D	A	B (T_{c2} = 40)
σ	[1$\bar{1}$0] [001] [110]	D	C	B (T_{c2} = 38)
σ	[001] [$\bar{1}$10] [110]	D	A	C
(σ = 0)	[100] [010] [001]	C	C	C
(σ = 0)	[110] [1$\bar{1}$0] [001]	C	C	C

FIG. 4: Crystal orientation dependence of skyrmion stability under uniaxial tensile strain. (a)-(d) Schematic illustration of typical H-T phase diagrams for strained and unstrained Cu_2OSeO_3. The SkX state is represented by a red-shaded region, with the lower critical temperature T_{c2}. (e) Summary of magnetic phase diagrams obtained with various directional combinations of H and σ under different crystal orientations. A, B, C, and D symbols represent the phase diagrams shown in (a)-(d), respectively.